

Chiral excitation of spin waves in ferromagnetic films

Tao Yu,¹ Chuanpu Liu,² Haiming Yu,² Yaroslav M. Blanter,¹ and Gerrit E. W. Bauer^{3,1}

¹*Kavli Institute of NanoScience, Delft University of Technology, 2628 CJ Delft, The Netherlands*

²*Fert Beijing Institute, BDBC, School of Microelectronics, Beihang University, Beijing 100191, China*

³*Institute for Materials Research & WPI-AIMR & CSRN, Tohoku University, Sendai 980-8577, Japan*
(Dated: November 19, 2021)

We theoretically investigate the interlayer dipolar and exchange couplings for an array of metallic magnetic nanowires grown on top of an extended ultrathin yttrium iron garnet film. The calculated interlayer dipolar coupling agrees with observed anticrossings [Chen *et al.*, Phys. Rev. Lett. **120**, 217202 (2018)], concluding that the interlayer exchange coupling is suppressed by a spacer layer between the nanowires and film. The Kittel mode in the nanowire array couples chirally to spin waves in the film, even though Damon-Eshbach surface modes do not exist. The chirality is suppressed when the interlayer exchange coupling becomes strong.

I. INTRODUCTION

Magnon spintronics is the research field aimed at understanding and controlling spin waves — the collective excitations of magnetic order — and its quanta, magnons, with perspectives of technological applications [1–4]. Yttrium iron garnet (YIG), a ferrimagnetic insulator, is currently the best material for magnon spintronics due to its record low damping [5–7]. Long-wavelength spin waves in YIG can travel over centimeters [8]. Dipolar interactions add unique features to the magnetostatic surface or Damon-Eshbach (DE) spin waves in magnetic film with in-plane magnetization that are exponentially localized at the surface and possess directional chirality: the surface spin waves propagate only in one direction that is governed by surface normal and magnetization directions [9–18]. This chirality can be very attractive for application in magnetic logics [19]. However, dipolar surface spin waves suffer from a low group velocity which makes them less attractive for information transfer. A different mechanism — exchange interactions — generates spin waves with much higher group velocity, but they are scattered easily. Transport is then slowed down by becoming diffusive and their reach becomes limited to the order of 10 μm and the directional chirality vanishes as well.

The spin waves most suitable for information technologies therefore arise in the intermediate regime, i.e., dipolar-exchange spin waves that combine the long-lifetime and attractive features, such as the chirality of magnetostatic magnons, with the higher group velocity generated when the exchange interaction kicks in. Unfortunately, these spin waves are hard to excite since coherent microwave absorption conserves linear momentum, and the impedance matching problem exists when using conventional coplanar waveguide. Recently, excitation of relatively-short-wavelength spin waves in Co(FeB)|YIG thin-film bilayers with uniform microwave fields has been demonstrated [20, 21], but these are standing waves which can not travel. Refs. [22, 23] demonstrated that microwaves can excite higher-momentum in-plane spin waves by ferromagnetic resonance (FMR) of Ni or Co

nanowire arrays (NWA) on an ultrathin (20 nm) YIG film (see Fig. 1). The dimensions of the grating in Fig. 1 are the thickness h and width d of the nanowires, the period or center-to-center distance between the nanowires a , and the YIG thickness s . We choose \hat{z} to be parallel to the nanowires, the magnetizations, and the applied magnetic field. A thin non-magnetic layer between the nanowires and film suppresses the interlayer exchange coupling. We allow NWA and YIG magnetizations to be antiparallel as well. We investigate the magnetization dynamics of such a magnetic grating on a magnetic film and find the spin waves can be chirally excited. This is at the first glance surprising since DE surface modes [10] do not exist for such thin films. However, it corresponds to and explains recent experiments (Yu *c.s.*, unpublished). We show that the chirality arises from the unique polarization-momentum locking of the dipolar field generated by the Kittel modes of NWA.

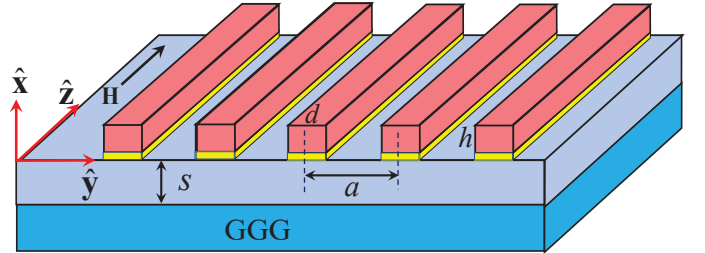


FIG. 1. Co or Ni nanowire grating on an YIG film with coordinate system and geometric parameters. The YIG film is fabricated on the gadolinium gallium garnet (GGG) substrate that is a non-magnetic insulator. A magnetic field is applied in the \hat{z} -direction, parallel to the nanowires. A thin non-magnetic spacer (yellow) may be inserted between the wires and the film to suppress the interface exchange interaction.

In the experiments, a coplanar waveguide on top of the NWA|YIG system of Fig. 1 is tuned to the NWA Kittel mode, in which the magnetization of all wires precesses in phase. Due to the large magnetization and form anisotropy of Co and Ni, this frequency is much higher

than that of the underlying YIG film FMR. The array acts as grating that couples to short-wavelength in-plane spin waves in the YIG film by the dipole and exchange couplings [22, 23]. Only the spin waves propagating perpendicular to the nanowires (the \hat{y} -direction in Fig. 1) with in-plane wave vector $\mathbf{k} = m\pi\hat{y}/a$ can be excited, where m is an even integer. The coherent coupling generates anti-crossings between the NWA Kittel mode and the spin waves in the YIG film that can be observed in the microwave reflection spectra [23]. The mode splitting is a direct measure of the interlayer coupling strength. Since YIG is magnetically very soft, the magnetizations of film and nanowires can be rotated with respect to each other, which enhances the interlayer coupling up to GHz when in antiparallel configuration [23]. We theoretically study the dynamics of this system, focussing on the experimentally relevant thin-YIG-film limit (e.g., $s \lesssim 20$ nm). We find a good agreement with experiments when only the dipolar coupling is taken into account, which could indicate that the spacer in the experiments suppresses the exchange interaction [23]. Interestingly, we find that the coupling is chiral, i.e. it excites only spin waves propagating with linear momentum $\mathbf{k} \parallel (\tilde{\mathbf{m}}_0 \times \mathbf{n})$, where $\tilde{\mathbf{m}}_0$ is the magnetization of and \mathbf{n} the normal to the film as is known for surface DE modes in thick films [10]. However, DE modes do not exist in thin films with a magnetization dynamics that is almost constant over the film thickness. The predicted chiral coupling of exchange spin waves survives a finite interface exchange coupling and adds functionality to down-scaled magnonic devices [24].

This paper is organized as follows. We first introduce the uncoupled modes for NWA and the YIG film in Sec. II. Then, the interlayer dipolar and exchange interactions are addressed in Sec. III followed by concrete calculations and comparison with experiments in Sec. IV. Finally, section V contains a discussion of the results and conclusions.

II. UNCOUPLED DYNAMICS

In this section, we formulate the Kittel mode dynamics in a NWA as well as spin waves in the thin magnetic film. The collective mode in the NWA generates the high momentum Fourier components that couple to the exchange spin waves in the film as elaborated in Section III. There we also need the spin waves amplitude formulated in Section II B.

A. Kittel mode in nanowire array (NWA)

The NWA with a length much larger than the periodicity is to a very good approximation a one-dimensional magnonic crystal [1, 25–27]. In this limit we may disregard interwire dipolar interactions.

The frequency ω_K and magnetization amplitude $\mathbf{m}^K = (m_x^K, m_y^K)$ of the Kittel mode in a single magnetic wire read [28, 29]

$$\omega_K = \mu_0\gamma\sqrt{(H_{\text{app}} + M_0N_{xx})(H_{\text{app}} + M_0N_{yy})}, \quad (1)$$

$$m_y^K = i\sqrt{(H_{\text{app}} + M_0N_{xx})/(H_{\text{app}} + M_0N_{yy})}m_x^K, \quad (2)$$

where μ_0 is the vacuum permeability, $-\gamma$ the electron gyromagnetic ratio, H_{app} the applied magnetic field (in the \hat{z} -direction), M_0 the saturation magnetization, and $N_{\alpha\alpha}$ the demagnetization factor with $N_{zz} = 0$ for a sufficiently long wire [22, 28–32]. When $h \ll d$ (or $h \gg d$) the demagnetization factor of ellipsoids [32] simplifies to $N_{xx} \simeq d/(h+d)$ and $N_{yy} \simeq h/(h+d)$ [28–30], while

$$\omega_K^{(W)} \rightarrow \omega_K^{(0)} \left(1 + \frac{1}{2} \left(\frac{\mu_0\gamma M_0}{\omega_K^{(0)}} \right)^2 \frac{h}{d} \right), \quad (3)$$

where $\omega_K^{(0)} = \mu_0\gamma\sqrt{(H_{\text{app}} + M_0)H_{\text{app}}}$ is the FMR frequency of the extended film.

Under FMR, the Kittel modes of all wires excited by a homogeneous microwave field that precess in phase. The magnetization $\mathbf{M}(\mathbf{r})$ is periodic in the direction perpendicular to the nanowires,

$$\mathbf{M}(\mathbf{r}, t) = \begin{cases} \mathbf{M}(t), & y \in [na - \frac{d}{2}, na + \frac{d}{2}], x \in [0, h] \\ 0, & \text{otherwise} \end{cases}, \quad (4)$$

where n is an integer. The Fourier series of the transverse components of $\mathbf{M}(\mathbf{r})$ reads

$$M_\beta^K(\mathbf{r}, t) = m_\beta^K e^{-i\omega_K t} \Theta(h-x)\Theta(x) \sum_{m \geq 0}^{\text{even}} 2f_m \cos k_y^{(m)} y, \quad (5)$$

in which $\beta = \{x, y\}$, $\Theta(x)$ is the Heavyside step function, $k_y^{(m)} = m\pi/a$ with m a positive *even* integer and

$$f_m = \left(1 - \frac{1}{2}\delta_{m0} \right) \frac{2}{\pi m} \sin \left(\frac{d}{2} k_y^{(m)} \right). \quad (6)$$

$M_\beta^K(\mathbf{r})$ is the lowest acoustic mode with frequency ω_K for the nanowire array in the interval $\omega_K^{(0)} \leq \omega_K \leq \omega_K^{(W)}$ with $\omega_K^{(W)} - \omega_K^{(0)} = O(h/d)$ [1, 25, 26]. The normalization condition of the amplitudes read (for general modes labelled by p) [9, 27]

$$\int d\mathbf{r} [M_x^{(p)}(\mathbf{r})\overline{M_y^{(p)}(\mathbf{r})} - \overline{M_x^{(p)}(\mathbf{r})}M_y^{(p)}(\mathbf{r})] = -i/2, \quad (7)$$

where $\overline{M} = M^*$. The acoustic mode in Eq. (5) is elliptically polarized as

$$m_x^K = \sqrt{\frac{a}{4hd} \sqrt{\frac{H_{\text{app}} + M_0N_{yy}}{H_{\text{app}} + M_0N_{xx}}}} \\ \rightarrow \frac{1}{2d} \sqrt{\frac{ad}{h} \sqrt{\frac{H_{\text{app}}}{H_{\text{app}} + M_0}}} + O\left(\frac{h}{d}\right),$$

$$m_y^K = i \sqrt{\frac{a}{4hd} \sqrt{\frac{H_{\text{app}} + M_0 N_{xx}}{H_{\text{app}} + M_0 N_{yy}}}} \rightarrow \frac{i}{2d} \sqrt{\frac{ad}{h} \sqrt{\frac{H_{\text{app}} + M_0}{H_{\text{app}}}}} + O\left(\frac{h}{d}\right), \quad (8)$$

which can be strongly elliptic in the thin film limit.

B. Spin waves in a thin magnetic film

Magnetic modes $\tilde{\mathbf{M}}$ in the film are the solution of the Landau-Lifshitz (LL) equation [33]

$$d\tilde{\mathbf{M}}/dt = -\mu_0\gamma\tilde{\mathbf{M}} \times (\mathbf{H}_{\text{app}} + \tilde{\mathbf{H}}_d + \tilde{\mathbf{H}}_{\text{ex}}), \quad (9)$$

where $\mathbf{H}_{\text{app}} = H_{\text{app}}\hat{\mathbf{z}}$ is the same applied magnetic field as above, $\tilde{\mathbf{H}}_d$ is the dipolar field (see Appendix A) [34], and the exchange field $\tilde{\mathbf{H}}_{\text{ex}} = \alpha_{\text{ex}} \left(\partial_x^2 \tilde{\mathbf{M}} + \partial_y^2 \tilde{\mathbf{M}} + \partial_z^2 \tilde{\mathbf{M}} \right)$ with stiffness α_{ex} . We choose free boundary conditions $d\tilde{\mathbf{M}}(\mathbf{r})/dx|_{x=0,-s} = 0$ for simplicity [35–37], since the lowest mode in sufficiently thin films is not affected by partial pinning [38–41].

By translational symmetry in the $\hat{\mathbf{y}}\text{-}\hat{\mathbf{z}}$ plane, $\tilde{M}_{x,y}(\mathbf{r}) = \tilde{m}_{x,y}^{\mathbf{k}}(x) e^{ik_y y + ik_z z} e^{-i\omega t}$ with $\mathbf{k} \equiv k_y \hat{\mathbf{y}} + k_z \hat{\mathbf{z}}$. We focus on the spin waves with $k_z = 0$ that couple to the acoustic mode of the nanowire array (see Sec. III). From Eqs. (9) and (A3), $\tilde{m}_{\pm}^{k_y}(x) = \tilde{m}_{\pm}^{k_y}(x) \pm i\tilde{m}_{\pm}^{k_y}(x)$ and $d\tilde{m}_{\pm}^{k_y}(x)/dx|_{x=0,-s} = 0$, we have the Fourier series [17, 34]

$$\tilde{m}_{\pm}^{k_y}(x) = \sum_{l=0}^{\infty} (\sqrt{2}/\sqrt{1+\delta_{l0}}) \tilde{m}_{l,\pm}^{k_y} \cos \frac{l\pi x}{s}. \quad (10)$$

Eq. (9) leads to the following equations for $\tilde{m}_{l,\pm}^{k_y}$ [17, 34],

$$\begin{pmatrix} \tilde{\omega} + \Omega_H + \alpha_{\text{ex}} k_y^2 + \alpha_{\text{ex}} (l\pi/s)^2 + 1/2 & 1/2 - |k_y| Q_{ll}/2 \\ -1/2 + |k_y| Q_{ll}/2 & \tilde{\omega} - \Omega_H - \alpha_{\text{ex}} k_y^2 - \alpha_{\text{ex}} (l\pi/s)^2 - 1/2 \end{pmatrix} \begin{pmatrix} \tilde{m}_{l,+}^{k_y} \\ \tilde{m}_{l,-}^{k_y} \end{pmatrix} + \sum_{l' \neq l} \begin{pmatrix} 0 & -k_y \tilde{Q}_{ll'}/2 - |k_y| Q_{ll'}/2 \\ -k_y \tilde{Q}_{l'l}/2 + |k_y| Q_{l'l}/2 & 0 \end{pmatrix} \begin{pmatrix} \tilde{m}_{l',+}^{k_y} \\ \tilde{m}_{l',-}^{k_y} \end{pmatrix} = 0, \quad (11)$$

where $\tilde{\omega} \equiv \omega/(\mu_0\gamma\tilde{M}_0)$, $\Omega_H \equiv H_{\text{app}}/\tilde{M}_0$, and

$$Q_{ll'} = \frac{1}{s} \int_{-s}^0 dx \int_{-s}^0 dx' e^{-|x-x'| |k_y|} \cos\left(\frac{l'\pi}{s} x'\right) \cos\left(\frac{l\pi}{s} x\right) \frac{2}{\sqrt{(1+\delta_{l0})(1+\delta_{l'0})}},$$

$$\tilde{Q}_{ll'} = \frac{1}{s} \int_{-s}^0 dx \int_{-s}^0 dx' \text{sgn}(x-x') e^{-|x-x'| |k_y|} \cos\left(\frac{l'\pi}{s} x'\right) \cos\left(\frac{l\pi}{s} x\right) \frac{2}{\sqrt{(1+\delta_{l0})(1+\delta_{l'0})}}, \quad (12)$$

and $\text{sgn}(x-x') = 1$ when $x > x'$ and $\text{sgn}(x-x') = -1$ when $x < x'$.

The exchange energy for the spin waves along the $\hat{\mathbf{x}}$ -direction is $\alpha_{\text{ex}}(l\pi/s)^2$. For the typical film thickness $s \leq 20$ nm and magnon wavelength $2\pi/k_y \gtrsim 100$ nm,

$\alpha_{\text{ex}} k_y^2 \ll \alpha_{\text{ex}} (l\pi/s)^2$ when $l \geq 1$. In Appendix B, we argue that we may confine our attention to the spin waves in the lowest branch $l=0$ with amplitude governed by [17, 34]

$$\omega_0 \begin{pmatrix} \tilde{m}_{0,+}^{k_y} \\ \tilde{m}_{0,-}^{k_y} \end{pmatrix} = \mu_0\gamma\tilde{M}_0 \begin{pmatrix} -\Omega_H - \alpha_{\text{ex}} k_y^2 - \frac{1}{2} & \frac{1}{2} - \frac{1}{s|k_y|} \left(1 - \frac{1}{s|k_y|} e^{-s|k_y|}\right) \\ -\frac{1}{2} + \frac{1}{s|k_y|} \left(1 - \frac{1}{s|k_y|} e^{-s|k_y|}\right) & \Omega_H + \alpha_{\text{ex}} k_y^2 + \frac{1}{2} \end{pmatrix} \begin{pmatrix} \tilde{m}_{0,+}^{k_y} \\ \tilde{m}_{0,-}^{k_y} \end{pmatrix}, \quad (13)$$

which leads to the energy spectrum [34–37, 42]

$$\omega_0 = \mu_0\gamma\tilde{M}_0 [(\Omega_H + \alpha_{\text{ex}} k_y^2 + 1)(\Omega_H + \alpha_{\text{ex}} k_y^2) + \left(1 - \frac{1}{|k_y|s} + \frac{1}{|k_y|s} e^{-|k_y|s}\right) \left(\frac{1}{|k_y|s} - \frac{1}{|k_y|s} e^{-|k_y|s}\right)]^{\frac{1}{2}}. \quad (14)$$

and ellipticity

$$\tilde{m}_{0,y}^{k_y} = i \frac{F-1}{F+1} \tilde{m}_{0,x}^{k_y}, \quad (15)$$

where

$$F = \frac{-\frac{1}{2} + \frac{1 - \exp(-|k_y|s)}{|k_y|s}}{\frac{\omega_0}{\mu_0 \gamma \tilde{M}_0} - (\Omega_H + \alpha_{\text{ex}} k_y^2 + 1/2)}. \quad (16)$$

With the normalization Eq. (7) we find

$$\tilde{m}_{0,x}^{k_y} = \sqrt{\frac{F+1}{4s(F-1)}}, \quad \tilde{m}_{0,y}^{k_y} = i\sqrt{\frac{F-1}{4s(F+1)}}. \quad (17)$$

For wavelengths that are relatively short but still much larger than the film thickness or $s/\alpha_{\text{ex}} \lesssim |k_y| \lesssim 1/s$, the energy of the spin waves in the lowest branch approaches $\mu_0 \gamma \tilde{M}_0 \sqrt{(\Omega_H + \alpha_{\text{ex}} k_y^2 + 1)(\Omega_H + \alpha_{\text{ex}} k_y^2)}$, $|F| \gg 1$ and the precession becomes circular with $\tilde{m}_{0,y}^{k_y} = i\tilde{m}_{0,x}^{k_y} = i\sqrt{1/(4s)}$.

III. INTERLAYER DIPOLAR AND EXCHANGE INTERACTIONS

We now analyze the coupling between the NWA and film that generate the observed anticrossings in the microwave absorption. We focus on the experimental relevant interlayer dipolar and exchange couplings of the Kittel mode of the NWA and the spin waves in the lowest subband of the thin film. We adopt the configuration in which the equilibrium magnetizations and applied field are all parallel to the $\hat{\mathbf{z}}$ -direction. The results also hold for the antiparallel configuration with $\tilde{\mathbf{m}}_0 \parallel \mathbf{H}_{\text{app}} \parallel \hat{\mathbf{z}}$ and $\mathbf{M}_0 \parallel -\hat{\mathbf{z}}$, by replacing m_y^K with $-m_y^K$.

A. Interlayer dipolar interaction

The free energy due to the interlayer dipolar interaction reads [33]

$$\begin{aligned} F_d(t) &= -\mu_0 \int \tilde{\mathbf{M}}(\mathbf{r}, t) \cdot \mathbf{h}^D(\mathbf{r}, t) d\mathbf{r} \\ &= -\mu_0 \int \mathbf{M}^K(\mathbf{r}, t) \cdot \tilde{\mathbf{h}}^D(\mathbf{r}, t) d\mathbf{r}, \end{aligned} \quad (18)$$

where \mathbf{h}^D ($\tilde{\mathbf{h}}^D$) is the demagnetization field generated by the acoustic mode (spin waves) in the NWA (films) [33]

$$\begin{aligned} h_{\beta}^D(\mathbf{r}, t) &= \frac{1}{4\pi} \partial_{\beta} \int d\mathbf{r}' \frac{\partial_{\alpha} M_{\alpha}^K(\mathbf{r}', t)}{|\mathbf{r} - \mathbf{r}'|}, \\ \tilde{h}_{\beta}^D(\mathbf{r}, t) &= \frac{1}{4\pi} \partial_{\beta} \int d\mathbf{r}' \frac{\partial_{\alpha} \tilde{M}_{\alpha}(\mathbf{r}', t)}{|\mathbf{r} - \mathbf{r}'|}, \end{aligned} \quad (19)$$

where $\alpha, \beta = \{x, y\}$ and the repeated index implies summation (over α). The field acting on the nanowire array is $\tilde{\mathbf{h}}^D$ with $x > 0 > x'$ (see Fig. 1) while that acting on the film is \mathbf{h}^D with $x < 0$. Below, rich features are revealed for the interlayer dipolar coupling by both classical and quantum descriptions, which are further understood from the unique behaviors of \mathbf{h}^D and $\tilde{\mathbf{h}}^D$.

1. Classical description

In a classical description, the Kittel mode of the NWA as derived above reads (see Eq. (5))

$$\begin{aligned} \begin{pmatrix} M_x^K(\mathbf{r}, t) \\ M_y^K(\mathbf{r}, t) \end{pmatrix} &= \Theta(h-x)\Theta(x) \\ &\times \sum_{m \geq 0}^{\text{even}} 2f_m \cos(k_y^{(m)} y) \begin{pmatrix} m_x^K \cos(\omega_K t) \\ m_y^K \sin(\omega_K t) \end{pmatrix}. \end{aligned} \quad (20)$$

By substituting these modes into Eq. (19) and using the Coulomb integral

$$I = \int d\mathbf{r}' \frac{e^{ik_y y'} f(x')}{|\mathbf{r} - \mathbf{r}'|} = \frac{2\pi}{|k_y|} e^{ik_y y} \int dx' e^{-|x-x'| |k_y|} f(x'), \quad (21)$$

its dipolar field in the film below becomes

$$\begin{aligned} \begin{pmatrix} h_x^D(\mathbf{r}, t) \\ h_y^D(\mathbf{r}, t) \end{pmatrix} &= \sum_{m \geq 0}^{\text{even}} F_m e^{|k_y^{(m)}|x} \\ &\times \begin{pmatrix} \cos(k_y^{(m)} y) & -\sin(k_y^{(m)} y) \\ -\sin(k_y^{(m)} y) & -\cos(k_y^{(m)} y) \end{pmatrix} \begin{pmatrix} m_x^K \cos(\omega_K t) \\ m_y^K \sin(\omega_K t) \end{pmatrix}, \end{aligned} \quad (22)$$

with the form factor $F_m = f_m(1 - e^{-|k_y^{(m)}|h})$. By inspection of the dipolar fields under the wire center and between the wires

$$\mathbf{h}^D(x, y = 0, t) = \sum_{m \geq 0}^{\text{even}} F_m e^{|k_y^{(m)}|x} \begin{pmatrix} m_x^K \cos(-\omega_K t) \\ m_y^K \sin(-\omega_K t) \end{pmatrix}, \quad (23)$$

$$\mathbf{h}^D\left(x, y = \frac{a}{2}, t\right) = \sum_{m \geq 0}^{\text{even}} F_m (-1)^{\frac{m}{2}} e^{|k_y^{(m)}|x} \begin{pmatrix} m_x^K \cos(-\omega_K t) \\ m_y^K \sin(-\omega_K t) \end{pmatrix}, \quad (24)$$

it becomes clear that \mathbf{h}^D rotates in the x - y plane, but in opposite direction of \mathbf{M}^K . Decomposing the latter into right and left circularly-polarized components as $(m_x^K, m_y^K)^T = m_R^K(1, 1)^T + m_L^K(1, -1)^T$, the dipolar field Eq. (22) can be written

$$\begin{aligned} \begin{pmatrix} h_x^D(\mathbf{r}) \\ h_y^D(\mathbf{r}) \end{pmatrix} &= \sum_{m \geq 0}^{\text{even}} F_m e^{|k_y^{(m)}|x} \left[m_R^K \begin{pmatrix} \cos(-k_y^{(m)} y - \omega_K t) \\ \sin(-k_y^{(m)} y - \omega_K t) \end{pmatrix} \right. \\ &\left. + m_L^K \begin{pmatrix} \cos(k_y^{(m)} y - \omega_K t) \\ -\sin(k_y^{(m)} y - \omega_K t) \end{pmatrix} \right]. \end{aligned} \quad (25)$$

Since $k_y^{(m)} \geq 0$, the standing magnetization mode in the NWA generates two travelling dipolar field waves with opposite direction locked by the polarization. A right circularly polarized Kittel mode ($m_L^K = 0$) generates dipolar magnetic fields with the opposite polarization that propagate only in one direction, while ellipticity leads to

a second wave with same polarization sense but in opposite direction.

$\mathbf{h}^D(\mathbf{r})$ can now interact with the proximate spin waves in the film below, which we denote as

$$\tilde{\mathbf{M}}(\mathbf{r}, t) = \begin{pmatrix} \tilde{m}_x^{\mathbf{k}}(x) \cos(\mathbf{k} \cdot \mathbf{r}_{\parallel} - \omega t) \\ -\tilde{m}_y^{\mathbf{k}}(x) \sin(\mathbf{k} \cdot \mathbf{r}_{\parallel} - \omega t) \end{pmatrix}, \quad (26)$$

where $\mathbf{r}_{\parallel} = y\hat{\mathbf{y}} + z\hat{\mathbf{z}}$. Substituting, the magnetic free energy due to the interlayer dipolar coupling becomes

$$\begin{aligned} F_d(t) = & -\mu_0 \sum_{m \geq 0}^{\text{even}} F_m \int d\mathbf{r} e^{i k_y^{(m)} |x|} \\ & \times (\tilde{m}_x^{\mathbf{k}}(x) \cos(\mathbf{k} \cdot \mathbf{r}_{\parallel} - \omega t), -\tilde{m}_y^{\mathbf{k}}(x) \sin(\mathbf{k} \cdot \mathbf{r}_{\parallel} - \omega t)) \\ & \times \begin{pmatrix} \cos(k_y^{(m)} y) & -\sin(k_y^{(m)} y) \\ -\sin(k_y^{(m)} y) & -\cos(k_y^{(m)} y) \end{pmatrix} \begin{pmatrix} m_x^K \cos(\omega_K t) \\ m_y^K \sin(\omega_K t) \end{pmatrix}. \end{aligned} \quad (27)$$

The dipolar thin-film form anisotropy also causes elliptical precessions that can be decomposed into the right and left circularly-polarized components as $(\tilde{m}_x^{\mathbf{k}}(x), \tilde{m}_y^{\mathbf{k}}(x)) = \tilde{m}_R^{\mathbf{k}}(x)(1, 1) + \tilde{m}_L^{\mathbf{k}}(x)(1, -1)$. At resonance $\omega = \omega_K$ the average \bar{F}_d over a time period $2\pi/\omega_K$ is finite

$$\begin{aligned} \bar{F}_d = & -\mu_0 \sum_{m \geq 0}^{\text{even}} F_m \int dx e^{i k_y^{(m)} |x|} \\ & \times (\tilde{m}_R^{k_y}(x) m_L^K \delta_{k_y, k_y^{(m)}} + \tilde{m}_L^{k_y}(x) m_R^K \delta_{k_y, -k_y^{(m)}}) \end{aligned} \quad (28)$$

Eq. (28) leads to the following conclusions:

- The ac dipolar magnetic fields couple only to spin waves with the same polarization (conservation of angular momentum).
- The FMR resonance of the NWA couples only to spin waves with momentum $\pm k_y^{(m)} \hat{\mathbf{y}}$ (conservation of linear momentum).
- Circularly polarized excitations in both NWA and film do not interact when equilibrium magnetizations are parallel. However, they do couple in the antiparallel configuration, which is obtained from Eq. (28) by exchanging $\tilde{m}_R^{k_y} \leftrightarrow \tilde{m}_L^{k_y}$.
- When the spin waves are circularly polarized, i.e. $\tilde{m}_L^{k_y} = 0$, but the NWA modes are elliptic, the coupling is perfectly chiral, i.e. the Kittel mode of the NWA interacts with spin waves that propagate in one direction only.
- A finite chirality persists when both the spin waves and NWA mode are elliptically polarized as long as $\tilde{m}_R^{k_y^{(m)}}(x) m_L^K \neq \tilde{m}_L^{-k_y^{(m)}}(x) m_R^K$.

The dipolar (magnetostatic) spin waves in thin films are elliptically polarized due to the anisotropy of demagnetization fields, with the exception of the DE modes in thick films as discussed briefly below. The NWA Kittel mode then asymmetrically mixes with spin waves in both directions. At higher frequencies the dipolar interaction becomes less dominant and the spin waves become nearly circularly polarized, $\tilde{m}_L^{k_y} \rightarrow 0$, which implies that only spin waves propagating in one direction interact as long as $m_L^K \neq 0$. When the magnetizations are antiparallel, m_R^K and m_L^K are exchanged, leading to perfect and large chiral coupling for circularly polarized magnetization dynamics.

The physics can be also understood in terms of the dipolar field generated by the spin waves and acting on the NWA. We can express the spin waves in the thin film as

$$\begin{pmatrix} \tilde{M}_x(\mathbf{r}) \\ \tilde{M}_y(\mathbf{r}) \end{pmatrix} = \tilde{m}_R(x) \begin{pmatrix} \cos(k_y y - \omega t) \\ -\sin(k_y y - \omega t) \end{pmatrix} + \tilde{m}_L(x) \begin{pmatrix} \cos(k_y y - \omega t) \\ \sin(k_y y - \omega t) \end{pmatrix}, \quad (29)$$

where $\tilde{m}_R(x)$ and $\tilde{m}_L(x)$ denote the right and left circularly-polarized components. Above the film with $x > 0 > x'$,

$$\begin{pmatrix} \tilde{h}_x^D(\mathbf{r}) \\ \tilde{h}_y^D(\mathbf{r}) \end{pmatrix} = \frac{1}{2} e^{-|k_y| x} \int dx' [(k_y + |k_y|) m_R(x') + (k_y - |k_y|) m_L(x')] \begin{pmatrix} \cos(k_y y - \omega t) \\ \sin(k_y y - \omega t) \end{pmatrix}. \quad (30)$$

Irrespective of an ellipticity \tilde{m}_L , the dipolar field is left (right) circularly polarized above (below) the film. Moreover, the dipolar field generated by the right (left) circularly polarized components of the spin waves does not vanish above the film only when $k_y > 0$ ($k_y < 0$). This can be understood in terms of the surface magnetic charges with dipolar fields that point in opposite direction on both sides of the film: When the spin waves are right or left circularly polarized, only those travelling in particular direction can couple with the NWA Kittel mode with fixed circularly polarized component.

Although not treated here explicitly, we can draw some conclusions about the DE modes in thick films as well. DE modes propagating perpendicular to the magnetization can be excited efficiently by interlayer dipolar coupling because they are circularly polarized, but the excitation efficiency is very different for the parallel and anti-parallel configurations. Here, we disregard the DE modes on the opposite side completely now since the film is thick. From Eq. (25), the anisotropic NWA generates the right (left) circularly polarized magnetic fields propagating in (opposite to) the $\hat{\mathbf{y}}$ -direction determined by m_L^K (m_R^K). With this in mind, DE modes of thick films can be efficiently excited by dipolar interactions because they are confined to a thin skin near the surface. However, the exchange coupling can also do that, irrespective of the parallel vs. antiparallel configuration but with equal

excitation efficiency. The NWA therefore can be an efficient coupler to excite short-wavelength DE modes that by the exchange interaction acquire a significant group velocity.

2. Quantum description

We now formulate the interlayer dipolar coupling in second quantization deriving the appropriate matrix elements from the classical interactions. In order to make better contact with the literature, we replace the magnetization $\mathbf{M}(\mathbf{r})$ by the spin operators $\hat{\mathbf{S}}(\mathbf{r})$ via $\mathbf{M}(\mathbf{r}) \rightarrow -\gamma\hbar\hat{\mathbf{S}}(\mathbf{r})$. After performing the Holstein-Primakoff transformation [28, 43], we linearize the problem in the magnon operators and diagonalize the resulting Hamiltonian by a Bogoliubov transformations [28, 43–45]. The leading term of the interaction between NWA and film then reads

$$\hat{H}_d = -\mu_0\gamma^2\hbar^2 \frac{1}{4\pi} \int d\mathbf{r} \hat{\mathbf{S}}_\alpha(\mathbf{r}) \partial_\beta \int d\mathbf{r}' \frac{\partial_\alpha \hat{\mathbf{S}}_\alpha^K(\mathbf{r}')}{|\mathbf{r} - \mathbf{r}'|}. \quad (31)$$

with spin operators (for the time being for general film thickness) [28, 43, 44],

$$\begin{aligned} \hat{S}_\gamma(\mathbf{r}, t) &= \sqrt{2\tilde{S}} \sum_{j\mathbf{k}} \left(\tilde{M}_\gamma^{(j\mathbf{k})}(\mathbf{r}) \hat{\alpha}_{j\mathbf{k}}(t) + \overline{\tilde{M}_\gamma^{(j\mathbf{k})}}(\mathbf{r}) \hat{\alpha}_{j\mathbf{k}}^\dagger(t) \right), \\ \hat{S}_\delta(\mathbf{r}, t) &= \sqrt{2S} \sum_p \left(M_\delta^{(p)}(\mathbf{r}) \hat{\beta}_p(t) + \overline{M_\delta^{(p)}}(\mathbf{r}) \hat{\beta}_p^\dagger(t) \right), \end{aligned} \quad (32)$$

with $\gamma, \delta = \{x, y\}$. Here $\hat{\alpha}_{j\mathbf{k}}$ is a magnon annihilation operator with band index j in the film and the Kittel mode of the nanowire array is annihilated by $\hat{\beta}_K$. Then

$$\begin{aligned} \hat{H}_d &= -\mu_0\gamma\hbar^2 \sqrt{\tilde{M}_0 M_0} \\ &\times \sum_{j\mathbf{k}} \left(\tilde{B}_{j\mathbf{k},K} \hat{\beta}_{j\mathbf{k}} \hat{\alpha}_{j\mathbf{k}}^\dagger + \tilde{A}_{j\mathbf{k},K} \hat{\beta}_{j\mathbf{k}} \hat{\alpha}_{j\mathbf{k}} + \text{h.c.} \right), \end{aligned} \quad (33)$$

in terms of

$$\begin{aligned} \tilde{B}_{j\mathbf{k},K} &= \sum_m F_m \int d\mathbf{r} e^{ik_y^{(m)}x} \tilde{\mathcal{M}}_{j\mathbf{k}}(\mathbf{r}) \left(\mathcal{Q}_{k_y^{(m)}} + \overline{\mathcal{Q}_{k_y^{(m)}}} \right) \overline{\mathcal{N}^K}, \\ \tilde{A}_{j\mathbf{k},K} &= \sum_m F_m \int d\mathbf{r} e^{ik_y^{(m)}x} \tilde{\mathcal{M}}_{j\mathbf{k}}(\mathbf{r}) \left(\mathcal{Q}_{k_y^{(m)}} + \overline{\mathcal{Q}_{k_y^{(m)}}} \right) \mathcal{N}^K. \end{aligned} \quad (34)$$

Here, $F_m = f_m(1 - e^{-k_y^{(m)}h})$, $\tilde{\mathcal{M}}_{j\mathbf{k}}(\mathbf{r}) = \left(\tilde{M}_x^{(j\mathbf{k})}(\mathbf{r}), \tilde{M}_y^{(j\mathbf{k})}(\mathbf{r}) \right)$, $\mathcal{N}^K = (m_x^K, m_y^K)^T$, and

$$\mathcal{Q}_{k_y^{(m)}} = e^{ik_y^{(m)}y} \begin{pmatrix} 1 & i \\ i & -1 \end{pmatrix}. \quad (35)$$

and calligraphic letters denote matrices here and below.

Only terms with $|k_y| = k_y^{(m)}$ survive the spatial integration in Eq. (34), which reflects momentum conservation. In the following, we focus again on the experimental

relevant regime [22, 23] of spin waves in the lowest branch $j = 0$, labeled in the following by ‘‘H’’ and the acoustic mode ‘‘K’’ in the nanowire array. With $\tilde{M}_\beta^{\mathbf{H},\mathbf{k}} = \tilde{m}_{0,\beta}^{\mathbf{k}} e^{i\mathbf{k}\cdot\mathbf{r}}$

$$\begin{aligned} \hat{H}_d &= \sum_m \left(D_d^m \hat{\beta}_{\mathbf{H},-k_y^{(m)}} \hat{\alpha}_{\mathbf{K}}^\dagger + C_d^m \hat{\beta}_{\mathbf{H},k_y^{(m)}} \hat{\alpha}_{\mathbf{K}}^\dagger \right. \\ &\left. + A_d^m \hat{\beta}_{\mathbf{H},-k_y^{(m)}} \hat{\alpha}_{\mathbf{K}} + B_d^m \hat{\beta}_{\mathbf{H},k_y^{(m)}} \hat{\alpha}_{\mathbf{K}} + \text{h.c.} \right), \end{aligned} \quad (36)$$

in which

$$\begin{aligned} D_d^m &= -\mu_0\gamma\hbar^2 \sqrt{\tilde{M}_0 M_0} F_m \int dx e^{k_y^{(m)}x} \mathcal{P}_{-k_y^{(m)}}(x) \overline{\mathcal{T} \mathcal{N}^K}, \\ C_d^m &= -\mu_0\gamma\hbar^2 \sqrt{\tilde{M}_0 M_0} F_m \int dx e^{k_y^{(m)}x} \mathcal{P}_{k_y^{(m)}}(x) \overline{\mathcal{T} \mathcal{N}^K}, \\ A_d^m &= -\mu_0\gamma\hbar^2 \sqrt{\tilde{M}_0 M_0} F_m \int dx e^{k_y^{(m)}x} \mathcal{P}_{-k_y^{(m)}}(x) \mathcal{T} \mathcal{N}^K, \\ B_d^m &= -\mu_0\gamma\hbar^2 \sqrt{\tilde{M}_0 M_0} F_m \int dx e^{k_y^{(m)}x} \mathcal{P}_{k_y^{(m)}}(x) \mathcal{T} \mathcal{N}^K, \end{aligned} \quad (37)$$

with the spinor

$$\mathcal{P}_{\pm k_y^{(m)}}(x) = \left(\tilde{m}_{0,x}^{\pm k_y^{(m)}}(x), \tilde{m}_{0,y}^{\pm k_y^{(m)}}(x) \right) \quad (38)$$

and

$$\mathcal{T} = \begin{pmatrix} 1 & i \\ i & -1 \end{pmatrix}. \quad (39)$$

The equilibrium magnetization of the NWA and film are parallel to the $\hat{\mathbf{z}}$ -direction. When they are antiparallel with $\tilde{\mathbf{m}}_0 \parallel \mathbf{H}_{\text{app}} \parallel \hat{\mathbf{z}}$ and $\mathbf{M}_0 \parallel -\hat{\mathbf{z}}$, m_y^K should be replaced by $-m_y^K$, as before.

We emphasize again that the couplings of the spin waves of opposite momentum to the acoustic Kittel mode in the NWA can be very different. When the wavelength is relatively short, or $|k_y| \gtrsim s/\alpha_{\text{ex}}$, the spin waves are nearly circularly polarized, $\tilde{m}_{0,y}^{\pm k_y^{(m)}} \approx i\tilde{m}_{0,x}^{\pm k_y^{(m)}}$. When substituted into D_d^m , the integral

$$\int dx e^{k_y^{(m)}x} \tilde{m}_{0,x}^{-k_y^{(m)}}(1, i) \begin{pmatrix} 1 & i \\ i & -1 \end{pmatrix} \begin{pmatrix} \overline{m_x^K} \\ \overline{m_y^K} \end{pmatrix} = 0 \quad (40)$$

and $D_d^m \approx A_d^m \approx 0$ in Eq. (37). This implies that the dipolar interaction cannot couple spin waves with momentum $-|k_y^{(m)}| \hat{\mathbf{y}}$ to the acoustic mode in the nanowire, while such a restriction does not hold for waves with $+|k_y^{(m)}| \hat{\mathbf{y}}$. In other words, the microwave field couples to short-wavelength spin waves in thin films via a nanowire grating in a chiral manner.

As discussed above, the physical reason for this unexpected selection rule is the asymmetry of the dipolar field generated by (circularly polarized) spin waves propagating normal to the magnetization ($\parallel \hat{\mathbf{y}}$). For a particular

momentum $q_y \hat{\mathbf{y}}$, the dipolar field generated by the circular spin waves on the upper side is

$$\begin{pmatrix} \tilde{h}_x^D(\mathbf{r}) \\ \tilde{h}_y^D(\mathbf{r}) \end{pmatrix} = \frac{e^{-|\mathbf{q}|x}}{2} e^{-i\omega_{\mathbf{q}}t} \int dx' e^{-|\mathbf{q}|x'} \begin{pmatrix} |q_y| & -iq_y \\ -iq_y & -|q_y| \end{pmatrix} \\ \times \begin{pmatrix} 1 \\ i \end{pmatrix} \tilde{M}_x(x', y, z), \quad (41)$$

which vanishes for negative q_y but is finite for positive q_y . Therefore only spin waves with positive (negative) q_y can couple (not couple) with the magnetization in the nanowire array.

The different excitation configurations and the chiral coupling are illustrated by Fig. 2. When the nanowire array is fabricated on the upper surface of the film, irrespective of whether the magnetizations in the film and nanowires are parallel [Fig. 2(a)] or anti-parallel [Fig. 2(b)], among the short-wavelength spin waves only those with momentum $\mathbf{k} \parallel (\tilde{\mathbf{m}}_0 \times \mathbf{n})$ (shown by the wavy line with arrow) couple to (are excited by) the acoustic NWA mode.

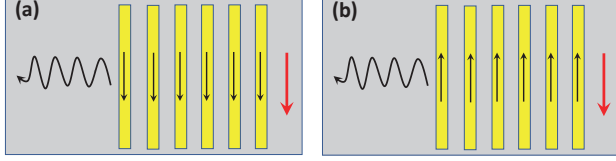


FIG. 2. Chiral coupling of spin waves due to the interlayer dipolar interaction for parallel and antiparallel magnetizations. The gray and yellow regions denote the film and nanowire array. The red and black arrows represent the direction of the soft magnetizations of the film in parallel to the external field and NWA, respectively. The wavy line with arrow indicates the propagating direction of spin waves that couple to the Kittel mode of the NWA.

B. NWA-magnetic film exchange interaction

Both the static [46–48] and dynamic [20, 21, 49–51] interlayer exchange interaction between the NWA and magnetic film can play a role in the coupling of short-wavelength spin waves in magnetic bilayers [20, 21, 50]. Here we focus on the dynamic exchange interaction, eventually moderated by spin diffusion in a spacer layer [20, 21, 49, 51, 52]. Indeed, recent experiments [21] show that for direct contact between Co and YIG bilayers, the static interfacial exchange interaction plays a dominant role by locking the interface magnetization on both sides together. A 5-nm Cu space layer, on the other hand, completely suppresses the static exchange interaction, while the dynamic interaction mediated by the exchange of non-equilibrium spin currents through the spacer remains [21]. A 1.5-nm AlO_x layer suppresses both static

and dynamic exchange interactions [21]. Here, we assess the role of a significant direct exchange interaction between the NWA and film, but do not discuss the dissipative dynamic coupling.

The free energy due to an interfacial exchange interaction density J can be written as [21, 46–48]

$$\begin{aligned} F_{\text{ex}} &= \int d\mathbf{r} J \delta(x) \tilde{\mathbf{M}}(\mathbf{r}) \cdot \mathbf{M}(\mathbf{r}) \\ &= J \int dy dz \tilde{\mathbf{M}}(x=0, y, z) \cdot \mathbf{M}(x=0, y, z), \quad (42) \end{aligned}$$

When $J > 0$ ($J < 0$), the interlayer exchange interaction is anti-ferromagnetic (ferromagnetic). J can be calculated by first principles [53] or fitted to experiments [20, 21, 23, 46, 47].

$$\hat{H}_{\text{ex}} = J \gamma^2 \int dy dz \hat{\mathbf{S}}(x=0, y, z) \cdot \hat{\mathbf{S}}(x=0, y, z). \quad (43)$$

As above, $\hat{\mathbf{S}}(x=0, y, z)$ and $\hat{\mathbf{S}}(x=0, y, z)$ represent the lowest spin wave subband in the film and the Kittel mode of the NWA. The expansion into normal modes, Eq. (32),

$$\begin{aligned} \hat{H}_{\text{ex}} &= \sum_m \left\{ D_{\text{ex}}^m \hat{\beta}_{\text{H}-k_y^{(m)}} \hat{\alpha}_{\text{K}}^\dagger + C_{\text{ex}}^m \hat{\beta}_{\text{HK}_y^{(m)}} \hat{\alpha}_{\text{K}}^\dagger \right. \\ &\quad \left. + A_{\text{ex}}^m \hat{\beta}_{\text{H}-k_y^{(m)}} \hat{\alpha}_{\text{K}} + B_{\text{ex}}^m \hat{\beta}_{\text{H}-k_y^{(m)}} \hat{\alpha}_{\text{K}} + \text{h.c.} \right\}, \quad (44) \end{aligned}$$

then contains the coefficients

$$D_{\text{ex}}^m = 2J \sqrt{\tilde{M}_0 M_0} f_m \sum_{\beta=x,y} \tilde{m}_\beta^{-k_y^{(m)}} (x=0) \overline{m_{0,\beta}^{\text{K}}}, \quad (45)$$

$$C_{\text{ex}}^m = 2J \sqrt{\tilde{M}_0 M_0} f_m \sum_{\beta=x,y} \tilde{m}_\beta^{k_y^{(m)}} (x=0) \overline{m_{0,\beta}^{\text{K}}}, \quad (46)$$

$$A_{\text{ex}}^m = 2J \sqrt{\tilde{M}_0 M_0} f_m \sum_{\beta=x,y} \tilde{m}_\beta^{-k_y^{(m)}} (x=0) m_{0,\beta}^{\text{K}}, \quad (47)$$

$$B_{\text{ex}}^m = 2J \sqrt{\tilde{M}_0 M_0} f_m \sum_{\beta=x,y} \tilde{m}_\beta^{k_y^{(m)}} (x=0) m_{0,\beta}^{\text{K}}. \quad (48)$$

For short-wavelength spin waves with nearly constant amplitude across a thin film, $D_{\text{ex}}^m \approx C_{\text{ex}}^m$ and $A_{\text{ex}}^m \approx B_{\text{ex}}^m$. The expressions above hold when magnetizations in the NWA and films are both parallel to the $\hat{\mathbf{z}}$ -direction. When they are anti-parallel $m_y^{\text{K}} \rightarrow -m_y^{\text{K}}$ in Eqs. (45–48).

C. Energy spectra of coupled NWA-spin wave modes

With established interlayer dipolar and exchange coupling between the lowest-branch spin waves in the film and acoustic mode in the nanowire array, we can compute the energy spectra of the coupled system.

1. Dominant interlayer dipolar coupling: anticrossings

We first focus on the interlayer dipolar interaction, assuming that the interlayer exchange interaction is efficiently suppressed by a thin spacer [20, 21]. We then may use the approximate selection rule found in Sec. III A: when $|k_y^m| \gtrsim s/\alpha_{\text{ex}}$, the interlayer dipolar coupling between the acoustic mode in the nanowire array and the short-wavelength spin waves is chiral. This simplifies the analysis since one only needs to consider the dipolar coupling between $\hat{\beta}_{\text{HK}_y^{(m)}}$ and $\hat{\alpha}_{\text{K}}$. For a particular $k_y^{(m)}$, the Hamiltonian of this subspace reads

$$\hat{H}(k_y^{(m)}) = (1/2)(\hat{\beta}_{\text{HK}_y^{(m)}}^\dagger, \hat{\alpha}_{\text{K}}, \hat{\beta}_{\text{HK}_y^{(m)}}, \hat{\alpha}_{\text{K}}^\dagger) \times \begin{pmatrix} \tilde{\omega}_{\text{HK}_y^{(m)}} & \overline{B}_d^m & 0 & \overline{C}_d^m \\ B_d^m & \omega_{\text{K}} & \overline{C}_d^m & 0 \\ 0 & C_d^m & \tilde{\omega}_{\text{HK}_y^{(m)}} & B_d^m \\ C_d^m & 0 & \overline{B}_d^m & \omega_{\text{K}} \end{pmatrix} \begin{pmatrix} \hat{\beta}_{\text{HK}_y^{(m)}} \\ \hat{\alpha}_{\text{K}}^\dagger \\ \hat{\beta}_{\text{HK}_y^{(m)}} \\ \hat{\alpha}_{\text{K}} \end{pmatrix}, \quad (49)$$

where $\tilde{\omega}_{\text{HK}_y^{(m)}}$ and ω_{K} are the energies of the lowest-branch spin waves with momentum $k_y^{(m)}\hat{y}$ and the NWA Kittel mode, respectively. When $|B_d^m| \ll \tilde{\omega}_{\text{HK}_y^{(m)}}, \omega_{\text{K}}$, terms with B_d^m may be disregarded from rotating wave approximation, the Hamiltonian is simplified to the quadratic form

$$\hat{H}(k_y^{(m)}) = (\hat{\beta}_{\text{HK}_y^{(m)}}^\dagger, \hat{\alpha}_{\text{K}}^\dagger) \begin{pmatrix} \tilde{\omega}_{\text{HK}_y^{(m)}} & \overline{C}_d^m \\ C_d^m & \omega_{\text{K}} \end{pmatrix} \begin{pmatrix} \hat{\beta}_{\text{HK}_y^{(m)}} \\ \hat{\alpha}_{\text{K}} \end{pmatrix}, \quad (50)$$

with the frequencies

$$\omega_{\pm}(k_y^{(m)}) = \frac{\tilde{\omega}_{\text{HK}_y^{(m)}} + \omega_{\text{K}}}{2} \pm \sqrt{\left(\frac{\tilde{\omega}_{\text{HK}_y^{(m)}} - \omega_{\text{K}}}{2}\right)^2 + |C_d^m|^2}. \quad (51)$$

$|C_d^m|$ is the coupling strength between the short-wavelength spin waves in the film and the acoustic mode in the nanowire array which governs the anticrossing with splitting of $2|C_d^m|$ between these modes at the resonance $\tilde{\omega}_{\text{HK}_y^{(m)}} = \omega_{\text{K}}$. In Sec. IV, we calculate this coupling strength for experimental conditions in Refs. [22, 23], which can be used to understand the experiments [22, 23] without having to invoke interface exchange.

2. Dominant interlayer exchange coupling: in-plane standing wave

When the interlayer exchange is active, we need to additionally consider the couplings between $\hat{\alpha}_{\text{K}}$, $\hat{\beta}_{\text{HK}_y^{(m)}}$ and $\hat{\beta}_{\text{H}-k_y^{(m)}}$. At resonance $\omega_{\text{K}} = \omega_{\text{H}\pm k_y^{(m)}} \equiv \omega_m^0$, the

Hamiltonian becomes

$$\hat{H} \approx (\hat{\alpha}_{\text{K}}^\dagger, \hat{\beta}_{\text{HK}_y^{(m)}}^\dagger, \hat{\beta}_{\text{H}-k_y^{(m)}}^\dagger) \begin{pmatrix} \omega_m^0 & C_m & D_m \\ C_m & \omega_m^0 & 0 \\ D_m & 0 & \omega_m^0 \end{pmatrix} \begin{pmatrix} \hat{\alpha}_{\text{K}} \\ \hat{\beta}_{\text{HK}_y^{(m)}} \\ \hat{\beta}_{\text{H}-k_y^{(m)}} \end{pmatrix}, \quad (52)$$

where $C_m = C_d^m + C_{\text{ex}}^m$ and $D_m = D_d^m + D_{\text{ex}}^m$. Its eigenvalues are

$$\begin{aligned} \omega_1 &= \omega_m^0, \\ \omega_2 &= \omega_m^0 - \sqrt{|C_m|^2 + |D_m|^2}, \\ \omega_3 &= \omega_m^0 + \sqrt{|C_m|^2 + |D_m|^2}, \end{aligned} \quad (53)$$

with corresponding eigenfunctions

$$\begin{aligned} \psi_1 &= (0, -D_m/C_m, 1), \\ \psi_2 &= \left(-\sqrt{|C_m|^2 + |D_m|^2}/D_m, C_m/D_m, 1\right), \\ \psi_3 &= \left(\sqrt{|C_m|^2 + |D_m|^2}/D_m, C_m/D_m, 1\right). \end{aligned} \quad (54)$$

When the interlayer exchange interaction is much larger than the dipolar one, $C_m \approx D_m$. In this situation, the first eigenfunction in Eq. (54) corresponds to the *in-plane standing wave* in the film, which arises from the linear superposition of the two spin waves with opposite momenta.

IV. MATERIAL AND DEVICE PARAMETER DEPENDENCE

In this section, we illustrate the expressions we produced above and demonstrate the magnitude of the effect by specifically considering coupling between a nanowire array and a thin film for the Co or Ni NWAs fabricated on YIG films. This system has been experimentally realized in Refs. [22, 23], and we use the parameters from these papers.

A. Co nanowire array

The lattice constant of the Co nanowire array was $a = 180$ nm with wire thickness $h = 20$ nm and width of $d = 132$ nm [22, 23]. The saturated magnetization $\mu_0 M_0 = 1.1$ T for the Co and $\mu_0 \tilde{M}_0 = 0.177$ T for the YIG films. The YIG exchange interaction constant is $\alpha_{\text{ex}} = 3 \times 10^{-16}$ m² [54] and thickness $s = 20$ nm [23]. We compute the coupling constants for these parameters when the magnetizations in the nanowire array and film are parallel and antiparallel to each other in Figs. 3(a) and (b), respectively, as a function of the mode index $m = \pi/(k_y^{(m)} a)$ of allowed spin waves in YIG. The magnetic field is chose to be constant and to agree with a main anticrossing. In Fig. 3(a), for example, $\mu_0 H_z = 0.012$ T corresponds to the anticrossing of the mode $m = 4$.

1. Parallel configuration

When $\mathbf{M}_0 \parallel \tilde{\mathbf{m}}_0 \parallel \mathbf{H}_{\text{app}} \parallel \hat{\mathbf{z}}$ the mode dependence of the dipolar coupling strengths is shown in Fig. 3(a) with applied magnetic fields $\mu_0 H_z = 0.012$ and 0.05 T. When $\mu_0 H_z = 0.012$ T, in Fig. 3(a), the blue (red) solid curve with squares (circles) describes the mode dependence of the interlayer dipolar coupling between the low-

est spin wave subband with momentum $k_y^{(m)} \hat{\mathbf{y}}$ ($-k_y^{(m)} \hat{\mathbf{y}}$) in the YIG film and the FMR of the Co nanowire array. The coupling strength for the spin waves with positive wave vector $k_y^{(m)} \hat{\mathbf{y}}$ is much larger than that for opposite $-k_y^{(m)} \hat{\mathbf{y}}$ one when $m \geq 4$ that corresponds to exchange spin waves, confirming that the chirality of the coupling should be very significant in real systems.

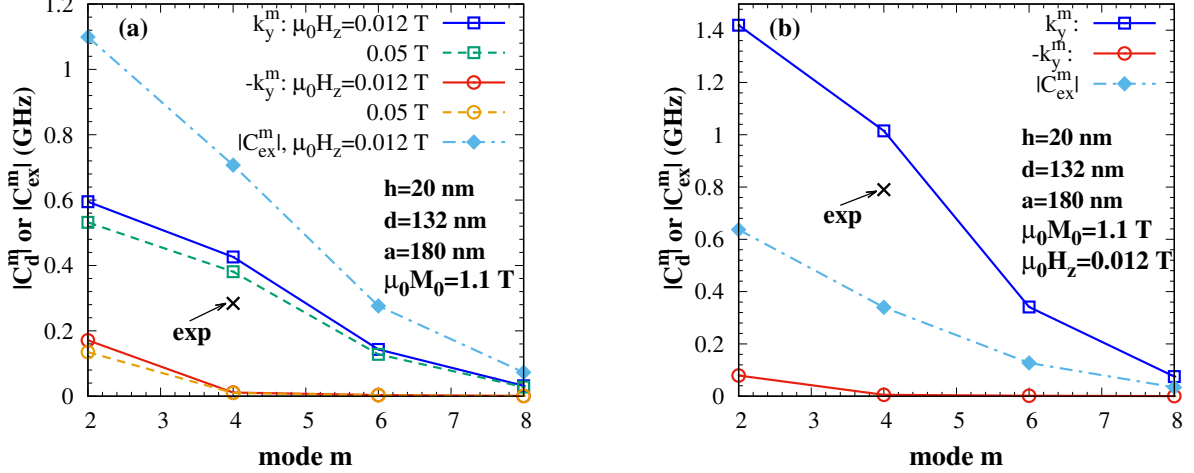


FIG. 3. (Color online) Mode dependence of the interlayer dipolar and exchange couplings between Co nanowires and a YIG film for parallel (a) and antiparallel (b) magnetizations. In (a) the blue (red) solid curve with squares (circles) represents the interlayer dipolar coupling between the spin waves with momentum $k_y^m \hat{\mathbf{y}}$ ($-k_y^{(m)} \hat{\mathbf{y}}$) in the film and the Kittel mode mode of the NWA for $\mu_0 H_z = 0.05$ T, while the cyan dot-dashed curve with diamonds denotes the interlayer exchange coupling (which is the same for spin wave directions). Analogous curves are plotted for $\mu_0 H_z = 0.012$ T (the exchange contribution does not depend on the field). The crosses in (a) and (b) denote the anticrossing gaps observed in FMR experiments [23]. m is an even integer.

With increasing mode number, the coupling strength decreases. According to Eq. (37), $C_d^m \propto F_m \int_{-s}^0 dx e^{k_y^{(m)} x}$, where F_m is the Fourier component of the NWA magnetization dynamics, while the integral represents the decay of the dipolar field inside the film. The drop of the coupling with increasing m is caused by the evanescent decay of the dipolar field and not by the form factor $F_m \propto \sin(k_y^{(m)} d/2)$. In the presence of a non-magnetic insertion with thickness δ , the overlap integral

$$\int_{-s-\delta}^{-s} dx e^{k_y^{(m)} x} = \int_{-s}^0 dx e^{k_y^{(m)} (x-\delta)} = e^{-k_y^m \delta} \int_{-s}^0 dx e^{k_y^{(m)} x}. \quad (55)$$

So the inserted layer exponentially suppresses the interlayer dipolar coupling by $e^{-k_y^m \delta}$. However, this effect is rather inefficient for $\delta = 1$ nm and a wave length $2\pi/k_y^m = 100$ nm, i.e. $k_y^m \delta = \pi/50 \approx 0.06$.

The decrease of the coupling with magnetic field in Fig. 3(a) can be understood as follows. For relatively short-wavelength spin waves with $\tilde{m}_{0,y}^{k_y^{(m)}} \approx i\tilde{m}_{0,x}^{k_y^{(m)}}$, Eq. (37) gives

$$C_d^m \approx -2\mu_0\gamma\sqrt{\tilde{M}_0 M_0} \frac{F_m}{k_y^m} (1 - e^{-k_y^{(m)} s}) \tilde{m}_{0,x}^{k_y^{(m)}} (m_x^K - i\overline{m_y^K}). \quad (56)$$

For $s/\alpha_{\text{ex}} \lesssim |k_y| \lesssim 1/s$ the amplitudes $\tilde{m}_{0,x}^{k_y^{(m)}}$ and $\tilde{m}_{0,y}^{k_y^{(m)}}$ in the film do not depend strongly on the field, in contrast to the NWA Kittel mode. Specifically,

$$-(m_x^K - i\overline{m_y^K}) = (\mathcal{F}^{1/4} - \mathcal{F}^{-1/4})\sqrt{a/(4hd)}, \quad (57)$$

in which $\mathcal{F} \equiv (H_{\text{app}}^z + M_0^z N_{xx}) / (H_{\text{app}}^z + M_0^z N_{yy})$. When $N_{xx} \gg N_{yy}$ and $M_0^z \gg H_{\text{app}}^z$, $\mathcal{F} \approx M_0^z N_{xx} / (H_{\text{app}}^z +$

$M_0^z N_{yy}$) decreases with H_{app}^z and so does the interlayer dipolar coupling.

We also present the interlayer exchange coupling $C_{\text{ex}}^{(m)}$ for direct contact between the Co NWA and the YIG film by the cyan dot-dashed curve with diamonds in Fig. 3(a), with an interlayer exchange coupling constant $J = 200 \mu\text{J}/\text{m}^2$ [21]. Without spacer layer, the interlayer exchange coupling wins over the dipolar interaction for the sample geometries considered here. The decrease can be understood from C_{ex}^m in Eq. (46): $\tilde{m}_{0,x}^{k_y^{(m)}}$, $\tilde{m}_{0,y}^{k_y^{(m)}}$, m_x^K and m_y^K do not depend strongly on mode number, but we find a decreasing $|C_{\text{ex}}^m| \propto |\sin(k_y^{(m)} d/2)/m|$ with increasing m . C_{ex}^m can also become oscillatory as a function of m (refer to Sec. IV B below).

2. Antiparallel configuration

Assuming that $\tilde{\mathbf{m}}_0 \parallel \mathbf{H}_{\text{app}} \parallel \hat{\mathbf{z}}$ and $\mathbf{M}_0 \parallel -\hat{\mathbf{z}}$, M_0^z becomes negative and m_y^K is replaced by $-m_y^K$ when calculating the interlayer dipolar and exchange couplings. The results in Fig. 3(b) for $\mu_0 H_z = 0.012$ T show a strong enhancement of the magnitude and chirality of the dipolar coupling at the cost of a reduced exchange interaction, which is caused by $|m_x^K - i\overline{m_y^K}| < |m_x^K + i\overline{m_y^K}|$, see Eq. (8). However, we disregarded here a possible exchange-spring magnetization texture in the non-collinear and antiparallel configurations [23], whose treatment is beyond of the scope of this work.

B. Ni nanowire array

Experiments have been also carried out on a Ni NWA with a (relatively large) lattice constant $a = 600$ nm, and thickness and width of $h = 20$ nm and $d = 258$ nm, respectively, and with a thin spacer of 1 nm between Ni wires and the YIG substrate [22, 23]. The Ni saturated magnetization is $\mu_0 M_0 = 0.6$ T [23]. For these parameter the factor $\sim \sin(k_y^{(m)} d/2)$ causes a non-monotonous dependence of the interlayer dipolar coupling, see Fig. 4. For $\mu_0 H_z = 0.015$ T, the asymmetry in the coupling of the Kittel mode to spin waves propagating into opposite directions is strong, for $m \geq 4$, the chirality is almost perfect. For larger $\mu_0 H_z = 0.11$ T the interlayer dipolar coupling is suppressed for the same reason as for the Co NWA discussed above.

The interlayer exchange coupling is also shown in Fig. 4 for an exchange interaction strength $J = 30 \mu\text{J}/\text{m}^2$ [23], which is smaller than the dipolar one.

C. Summary of the comparison with experiments

The present study was motivated by FMR experiments which displayed clear anti-crossings, i.e. strong

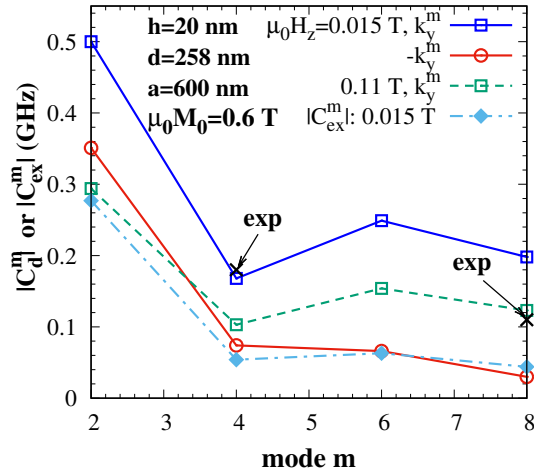


FIG. 4. (Color online) Mode dependences of the interlayer dipolar and exchange couplings between a Ni NWA and YIG film when magnetizations and applied field are all parallel along the wires. The blue solid curve with squares and red solid curve with circles represent the interlayer dipolar couplings for the spin waves with momenta $k_y^{(m)} \hat{\mathbf{y}}$ and $-k_y^{(m)} \hat{\mathbf{y}}$, respectively, for $\mu_0 H_z = 0.015$ T. The green dashed curve with squares is the interlayer dipolar coupling for positive momenta and $\mu_0 H_z = 0.11$ T. The cyan dot-dashed curve with diamonds denotes the interlayer exchange coupling for momenta $\pm k_y^{(m)} \hat{\mathbf{y}}$ when $\mu_0 H_z = 0.015$ T. The crosses are the mode splittings observed in the FMR [23].

coupling, between YIG film and NWA spin wave modes [22, 23]. The observed splittings are shown by the crosses in Figs. 3 and 4, respectively. The experimental values are quite close to the calculated ones for dipolar interactions without fit parameters. This supports the assumption that interlayer exchange interactions are suppressed by spacer layers inserted between the YIG film and Co/Ni nanowires [20–23]. A dominant interlayer dipolar interaction implies a chiral coupling. As shown in Figs. 3 and 4, only the short-wavelength spin waves propagating with momenta $\mathbf{k} \parallel \tilde{\mathbf{m}} \times \mathbf{n}$ interact with the NWA Kittel mode, where \mathbf{n} is the unit vector normal to the interface. A similar chiral feature is intrinsic to the Damon-Eshbach surface mode that exist in sufficiently thick films [10] but not in the ultrathin films considered here.

V. CONCLUSION AND DISCUSSION

In conclusion, we demonstrated that spin waves can be coherently excited in an ultrathin magnetic film in only one direction by a magnetic grating. We focus on the limiting cases in which the applied magnetic field and magnetizations in the film are either parallel or antiparallel

to the NWA magnetization and wire axis. We report an unexpected chirality in the coupling that strongly favors spin waves propagating perpendicular to the nanowires with wave vector $|\mathbf{k}| = m\pi/a$ (where m is an even integer and a the NWA lattice constant) [22, 23]. The dipolar regime can be realized by an inserted non-magnetic layer between the YIG film and nanowires that suppresses the exchange interaction more efficiently than the dipolar one [20, 21, 23]. The calculated coupling strength agrees well with the experimental observations [23] for both parallel and anti-parallel configurations. This suggests that the interlayer dipolar interaction plays a dominant role in the experiments [23], but more work, especially including magnetic texture and dynamic exchange is necessary to confirm this assertion. The spacer layer might also be instrumental to support an antiparallel magnetic configuration without associated exchange-spring magnetization textures in the film.

The dipolar coupling is a classical interaction between two magnetic bodies that has a relative longer range than the (static) exchange interaction. In the present configuration both interactions are exponentially suppressed with distance between the magnets, but on an atomic length scale and that of the wave length for exchange and dipolar coupling. In ultra-thin films without chiral surface waves, the exchange coupling mixes the Kittel mode almost symmetrically with the spin waves in opposite directions, thereby leading to in-plane *standing* waves by interference. In the presence of spacer layers, the dynamic exchange interaction competes as well, falling off on the scale of the spin-flip diffusion length, which can be rather long-range when the spacer is a clean simple metal such as copper [50].

The spin waves with the wave vector \mathbf{k} in a thin film with surface normal \mathbf{n} are coherently excited by the NWA grating with equilibrium magnetization along $\tilde{\mathbf{m}}$ and propagate dominantly in the direction $\mathbf{k} \parallel (\tilde{\mathbf{m}} \times \mathbf{n})$ (but only for significantly elliptic precession of either NWA or film magnetic modes). This phenomenology agrees with the intrinsic chirality of dipolar Damon-Eshbach surface modes in thick films [10]. However, the physics which we describe in this work is quite different, since there is no intrinsic chirality in the spin waves of ultrathin magnetic films with nearly constant amplitude over the film thickness. It is rather the intrinsic chirality of the dipolar fields that generates a chiral coupling to non-chiral spin waves. This directionality can be exploited in several ways [55], for example, to generate a heat conveyor belt [56–59] without the need for surface states.

Finally, we would point out an electric analogy, viz. the chiral coupling induced by rotating electric (rather than magnetic) dipoles. When excited close to a planar wave-

guide, the chiral evanescent electromagnetic field unidirectionally excites surface plasmon polaritons [60], also referred to as “spin-orbit interaction of light” [61]. There are large differences in the physics that we will emphasize elsewhere, but note that the dipolar field with momentum larger than ω/c with ω and c being the frequency and light velocity is evanescent on a sub-wavelength scale. Its chirality arises from the near-field interference of the radiated fields from the vertical and horizontal components of the ac electric field [60]. The circularly-polarized magnetic dipolar dynamics generates a purely circularly-polarized magnetic field [e.g., see Eq. (30)], while the circularly-polarized electric dipole results in an elliptically-polarized field by retardation [see Eq. (1) in Ref. [60]]. Nonetheless of this and other differences, the application perspective of the chiral coupling found in plasmonics such as broadband optical nanorouting [60, 61] and polarization analyzers [62] should stimulate similar activities in magnonics.

ACKNOWLEDGMENTS

This work is financially supported by the Nederlandse Organisatie voor Wetenschappelijk Onderzoek (NWO) as well as JSPS KAKENHI Grant No. 26103006. One of the authors (TY) would like to thank Sanchar Sharma and Jilei Chen for useful discussions.

Appendix A: Green function tensor

Here we review the calculation of the demagnetizing field [33]

$$\tilde{\mathbf{H}}_\beta^D = \frac{1}{4\pi} \partial_\beta \int \frac{\partial_\alpha \tilde{\mathbf{M}}_\alpha(\mathbf{r}')}{|\mathbf{r} - \mathbf{r}'|} d\mathbf{r}'. \quad (\text{A1})$$

in a thin magnetic film [34]. For a plane wave modulation $\tilde{\mathbf{M}}_\alpha(\mathbf{r}) = \tilde{\mathbf{m}}_\alpha(x) e^{ik_y y} e^{ik_z z}$,

$$\tilde{\mathbf{H}}_\beta^D = \frac{1}{2} \partial_\beta \left\{ \int_{-s}^0 dx' \left[-\tilde{\mathbf{m}}_x(x') \text{sgn}(x-x') + \tilde{\mathbf{m}}_y(x') \frac{ik_y}{|\mathbf{k}_\parallel|} + \tilde{\mathbf{m}}_z(x') \frac{ik_z}{|\mathbf{k}_\parallel|} \right] e^{-\text{sgn}(x-x')(x-x')|\mathbf{k}_\parallel|} e^{i\mathbf{k}_\parallel \cdot \mathbf{r}_\parallel} \right\}. \quad (\text{A2})$$

In matrix form

$$\begin{pmatrix} \tilde{\mathbf{H}}_x^D(\mathbf{r}) \\ \tilde{\mathbf{H}}_y^D(\mathbf{r}) \\ \tilde{\mathbf{H}}_z^D(\mathbf{r}) \end{pmatrix} = e^{i\mathbf{k}_\parallel \cdot \mathbf{r}_\parallel} \int_{-s}^0 dx' \mathcal{G}(x-x') \begin{pmatrix} \tilde{\mathbf{m}}_x(x') \\ \tilde{\mathbf{m}}_y(x') \\ \tilde{\mathbf{m}}_z(x') \end{pmatrix}, \quad (\text{A3})$$

where

$$\mathcal{G}(x-x') = e^{-|x-x'|\|\mathbf{k}_{\parallel}\|} \begin{pmatrix} \frac{\|\mathbf{k}_{\parallel}\|}{2} & -\frac{ik_y}{2} \text{sgn}(x-x') & -\frac{ik_z}{2} \text{sgn}(x-x') \\ -\frac{ik_y}{2} \text{sgn}(x-x') & -\frac{k_y^2}{2\|\mathbf{k}_{\parallel}\|} & -\frac{k_y k_z}{2\|\mathbf{k}_{\parallel}\|} \\ -\frac{ik_z}{2} \text{sgn}(x-x') & -\frac{k_y k_z}{2\|\mathbf{k}_{\parallel}\|} & -\frac{k_z^2}{2\|\mathbf{k}_{\parallel}\|} \end{pmatrix} - \delta_{\text{in}}(x-x') \mathcal{I} \quad (\text{A4})$$

is the Green function and \mathcal{I} the unity tensor. The δ_{in} -function vanishes when x lies outside the magnetic film. The demagnetization field $\tilde{\mathbf{H}}^D$ naturally satisfies electromagnetic boundary condition, i.e. continuity of the electromagnetic fields and currents at the surface of the magnet [34].

Appendix B: Higher magnon subbands in thin films

Here we estimate the effects of higher-order standing wave modes on the spin waves in the lowest subband.

Retaining only the lowest-order modes in Eq. (11) we arrive at the secular equation

$$\begin{pmatrix} \tilde{\omega} + \Omega_H + \alpha_{\text{ex}} k_y^2 + \frac{1}{2} & \frac{1}{2} - \frac{1}{2} |k_y| Q_{00} & 0 & -\frac{k_y}{2} \tilde{Q}_{01} - \frac{|k_y|}{2} Q_{01} \\ -\frac{1}{2} + \frac{1}{2} |k_y| Q_{00} & \tilde{\omega} - \Omega_H - \alpha_{\text{ex}} k_y^2 - \frac{1}{2} & -\frac{k_y}{2} \tilde{Q}_{01} + \frac{|k_y|}{2} Q_{01} & 0 \\ 0 & -\frac{k_y}{2} \tilde{Q}_{10} - \frac{|k_y|}{2} Q_{10} & \tilde{\omega} + \Omega_H + \alpha_{\text{ex}} k_y^2 + \alpha_{\text{ex}} \left(\frac{\pi}{s}\right)^2 + \frac{1}{2} & \frac{1}{2} - \frac{1}{2} |k_y| Q_{11} \\ -\frac{k_y}{2} \tilde{Q}_{10} + \frac{|k_y|}{2} Q_{10} & 0 & -\frac{1}{2} + \frac{1}{2} |k_y| Q_{11} & \tilde{\omega} - \Omega_H - \alpha_{\text{ex}} k_y^2 - \alpha_{\text{ex}} \left(\frac{\pi}{s}\right)^2 - \frac{1}{2} \end{pmatrix} \begin{pmatrix} \tilde{m}_{+,0} \\ \tilde{m}_{-,0} \\ \tilde{m}_{+,1} \\ \tilde{m}_{-,1} \end{pmatrix} = 0. \quad (\text{B1})$$

With Eq. (12) we find $Q_{01} = 0$ and $\tilde{Q}_{01} = 2\sqrt{2}s(e^{-|k_y|s} + 1)/(k_y^2 s^2 + \pi^2)$. The matrix in Eq. (B1) can be directly diagonalized by the Bogoliubov transformation [17]. We can use perturbation theory to estimate the importance of higher-order modes for our film thicknesses. The second mode contributes to the with am-

plitudes $c_k \equiv k_y \tilde{Q}_{01}/[2\alpha_{\text{ex}}(\pi/s)^2]$. For a grating with period $a = 180$ nm [22, 23], $k_y = 4\pi/a$, while thickness of the film is $s = 20$ nm. Then $k_y \tilde{Q}_{01}/2 = 0.208$, $\alpha_{\text{ex}}(\pi/s)^2 \approx 7.40$, and hence $c_k \approx 0.028$, which can be safely disregarded.

-
- ¹ B. Lenk, H. Ulrichs, F. Garbs, and M. Muenzenberg, Phys. Rep. **507**, 107 (2011).
 - ² A. V. Chumak, V. I. Vasyuchka, A. A. Serga, and B. Hillebrands, Nat. Phys. **11**, 453 (2015).
 - ³ D. Grundler, Phys. Rep. **11**, 407 (2016).
 - ⁴ V. E. Demidov, S. Urazhdin, G. de Loubens, O. Klein, V. Cros, A. Anane, and S. O. Demokritov, Phys. Rep. **673**, 1 (2017).
 - ⁵ V. Cherepanov, I. Kolokolov, and V. L'vov, Phys. Rep. **229**, 81 (1993).
 - ⁶ A. A. Serga, A. V. Chumak, and B. Hillebrands, J. Phys. D: Appl. Phys. **43**, 264002 (2010).
 - ⁷ M. Wu and A. Hoffmann, *Recent Advances in Magnetic Insulators: From Spintronics to Microwave Applications*, Vol. 64 (Elsevier, Amsterdam, 2013).
 - ⁸ A. A. Serga, A. V. Chumak, and B. Hillebrands, J. Phys. D **43**, 264002 (2010).
 - ⁹ L. R. Walker, Phys. Rev. **105**, 390 (1957).
 - ¹⁰ R. W. Damon and J. R. Eshbach, J. Phys. Chem. Solids **19**, 308 (1961).
 - ¹¹ A. Akhiezer, V. Bariakhtar, and S. Peletminski, *Spin Waves* (North-Holland, Amsterdam, 1968).
 - ¹² D. D. Stancil and A. Prabhakar, *Spin Waves—Theory and Applications* (Springer, New York, 2009).
 - ¹³ P. K. Amiria, B. Rejaei, M. Vroubel, and Y. Zhuang, Appl. Phys. Lett. **91**, 062502 (2007).
 - ¹⁴ T. Schneider, A. A. Serga, T. Neumann, B. Hillebrands, and M. P. Kostylev, Phys. Rev. B **77**, 214411 (2008).
 - ¹⁵ V. E. Demidov, M. P. Kostylev, K. Rott, P. Krzyszczyk, G. Reiss, and S. O. Demokritov, Appl. Phys. Lett. **95**, 112509 (2009).
 - ¹⁶ K. Sekiguchi, K. Yamada, S. M. Seo, K. J. Lee, D. Chiba, K. Kobayashi, and T. Ono, Appl. Phys. Lett. **97**, 022508 (2010).
 - ¹⁷ M. Kostylev, J. Appl. Phys. **113**, 053907 (2013).
 - ¹⁸ J. H. Kwon, J. Yoon, P. Deorani, J. M. Lee, J. Sinha, K. J. Lee, M. Hayashi, and H. Yang, Sci. Adv. **2**, 1501892 (2016).
 - ¹⁹ M. Jamali, J. H. Kwon, S.-M. Seo, K.-J. Lee, and H. Yang, Sci. Rep. **3**, 3160 (2013).
 - ²⁰ H. Qin, S. J. Hämäläinen, and S. van Dijken, Sci. Rep. **8**, 5755 (2018).

- ²¹ S. Klingler, V. Amin, S. Geprägs, K. Ganzhorn, H. Maier-Flaig, M. Althammer, H. Huebl, R. Gross, R. D. McMichael, M. D. Stiles, S. T. B. Goennenwein, and M. Weiler, *Phys. Rev. Lett.* **120**, 127201 (2018).
- ²² C. P. Liu, J. L. Chen, T. Liu, F. Heimbach, H. M. Yu, Y. Xiao, J. F. Hu, M. C. Liu, H. C. Chang, T. Stueckler, S. Tu, Y. G. Zhang, Y. Zhang, P. Gao, Z. M. Liao, D. P. Yu, K. Xia, N. Lei, W. S. Zhao, and M. Z. Wu, *Nat. Commun.* **9**, 738 (2018).
- ²³ J. L. Chen, C. P. Liu, T. Liu, Y. Xiao, K. Xia, G. E. W. Bauer, M. Z. Wu, and H. M. Yu, *Phys. Rev. Lett.* **120**, 217202 (2018).
- ²⁴ *Nanomagnetism and Spintronics*, edited by T. Shinjo (Elsevier, Oxford, 2009).
- ²⁵ A. V. Chumak, V. I. Vasyuchka, A. A. Serga, and B. Hillebrands, *Nat. Phys.* **11**, 453 (2015).
- ²⁶ A. V. Chumak, V. S. Tiberkevich, A. D. Karenowska, A. A. Serga, J. F. Gregg, A. N. Slavin, and B. Hillebrands, *Nat. Commun.* **1**, 141 (2010).
- ²⁷ R. Verba, G. Melkov, V. Tiberkevich, and A. Slavin, *Phys. Rev. B* **85**, 014427 (2012).
- ²⁸ C. Kittel, *Quantum Theory of Solids* (Wiley, New York, 1963).
- ²⁹ J. Ding, M. Kostylev, and A. O. Adeyeye, *Phys. Rev. B* **84**, 054425 (2011).
- ³⁰ C. Kittel, *Phys. Rev.* **73**, 155 (1948).
- ³¹ A. Aharoni, *J. Appl. Phys.* **83**, 3432 (1998).
- ³² J. A. Osborn, *Phys. Rev.* **67**, 351 (1945).
- ³³ L. D. Landau and E. M. Lifshitz, *Electrodynamics of Continuous Media*, 2nd ed. (Butterworth-Heinemann, Oxford, 1984).
- ³⁴ B. A. Kalinikos, *Sov. J. Phys.* **24**, 718 (1981).
- ³⁵ K. Yu. Guslienko, S. O. Demokritov, B. Hillebrands, and A. N. Slavin, *Phys. Rev. B* **66**, 132402 (2002).
- ³⁶ V. Vlaminck and M. Bailleul, *Phys. Rev. B* **81**, 014425 (2010).
- ³⁷ F. Zighem, Y. Roussigne, S.-M. Cherif, and P. Moch, *J. Phys.: Condens. Matter* **19**, 176220 (2007).
- ³⁸ R. E. De Wames and T. Wolfram, *Appl. Phys. Lett.* **15**, 297 (1969).
- ³⁹ T. Wolfram and R. E. De Wames, *Phys. Rev. Lett.* **24**, 1489 (1970).
- ⁴⁰ R. L. Stamps and B. Hillebrands, *Phys. Rev. B* **44**, 12417 (1991).
- ⁴¹ R. L. Stamps, *Phys. Rev. B* **49**, 339 (1994).
- ⁴² M. J. Hurben and C. E. Patton, *J. Magn. Magn. Mater.* **139**, 263 (1995).
- ⁴³ T. Holstein and H. Primakoff, *Phys. Rev.* **58**, 1098 (1940).
- ⁴⁴ A. Kamra and W. Belzig, *Phys. Rev. Lett.* **116**, 146601 (2016).
- ⁴⁵ S. Sharma, Y. M. Blanter, and G. E. W. Bauer, *Phys. Rev. B* **96**, 094412 (2017).
- ⁴⁶ P. Grünberg, R. Schreiber, Y. Pang, M. B. Brodsky, and H. Sowers, *Phys. Rev. Lett.* **57**, 2442 (1986).
- ⁴⁷ C. F. Majkrzak, J. W. Cable, J. Kwo, M. Hong, D. B. McWhan, Y. Yafet, J. V. Waszczak, and C. Vettier, *Phys. Rev. Lett.* **56**, 2700 (1986).
- ⁴⁸ M. D. Stiles, *J. Magn. Magn. Mater.* **200**, 322 (1999).
- ⁴⁹ Y. Tserkovnyak, A. Brataas, and G. E. W. Bauer, *Phys. Rev. Lett.* **88**, 117601 (2002).
- ⁵⁰ H. Skarsvåg, A. Kapelrud, and A. Brataas, *Phys. Rev. B* **90**, 094418 (2014).
- ⁵¹ T. Yu and M. W. Wu, *Phys. Rev. A* **92**, 013607 (2015).
- ⁵² B. Heinrich, Y. Tserkovnyak, G. Woltersdorf, A. Brataas, R. Urban, and G. E. W. Bauer, *Phys. Rev. Lett.* **90**, 187601 (2003).
- ⁵³ X. Jia, K. Liu, K. Xia, and G. E. W. Bauer, *Europhys. Lett.* **96**, 17005 (2011).
- ⁵⁴ S. Klingler, A. V. Chumak, T. Mewes, B. Khodadadi, C. Mewes, C. Dubs, O. Surzhenko, B. Hillebrands, and A. Conca, *J. Phys. D* **48**, 015001 (2015).
- ⁵⁵ T. Yu *et al.*, in preparation.
- ⁵⁶ T. An, V. I. Vasyuchka, K. Uchida, A. V. Chumak, K. Yamaguchi, K. Harii, J. Ohe, M. B. Jungfleisch, Y. Kajiwara, H. Adachi, B. Hillebrands, S. Maekawa, and E. Saitoh, *Nat. Mat.* **12**, 549 (2013).
- ⁵⁷ O. Wid, J. Bauer, A. Müller, O. Breitenstein, S. S. P. Parkin, and G. Schmidt, *Sci. Rep.* **6**, 28233 (2016).
- ⁵⁸ E. Shigematsu, Y. Ando, S. Dushenko, T. Shinjo, and M. Shiraishi, *Appl. Phys. Lett.* **112**, 212401 (2018).
- ⁵⁹ P. Wang, L. F. Zhou, S. W. Jiang, Z. Z. Luan, D. J. Shu, H. F. Ding, and D. Wu, *Phys. Rev. Lett.* **120**, 047201 (2018).
- ⁶⁰ F. J. Rodríguez-Fortuño, G. Marino, P. Ginzburg, D. O'Connor, A. Martínez, G. A. Wurtz, and A. V. Zayats, *Science* **340**, 328 (2013).
- ⁶¹ J. Petersen, J. Volz, and A. Rauschenbeutel, *Science* **346**, 67 (2014).
- ⁶² A. Espinosa-Soria, F. J. Rodríguez-Fortuño, A. Griol, and A. Martínez, *Nano Lett.* **17**, 3139 (2017).